J Nanopart Res (2010) 12:1137–1147
DOI 10.1007/s11051-009-9661-7

RESEARCH PAPER

High quality and tuneable silica shell–magnetic core nanoparticles

Carmen Vogt · Muhammet S. Toprak · Mamoun Muhammed · Sophie Laurent · Jean-Luc Bridot · Robert N. Müller

Received: 21 March 2009 / Accepted: 19 May 2009 / Published online: 3 June 2009

Abstract Obtaining small (<50 nm), monodispersed, well-separated, single iron oxide core–silica (SiO_2) shell nanoparticles for biomedical applications is still a challenge. Preferably, they are synthesised by inverse microemulsion method. However, substantial amount of aggregated and multicore core–shell nanoparticles is the undesired outcome of the method. In this study, we report on the production of less than 50 nm overall size, monodispersed, free of necking, single core iron oxide–SiO_2 shell nanoparticles with tuneable shell thickness by a carefully optimized inverse microemulsion method. The high degree of control over the process is achieved by understanding the mechanism of core–shell nanoparticles formation. By varying the reaction time and precursor concentration, the thickness of silica layer on the core nanoparticles can be finely adjusted from 5 to 13 nm. Residual reactions during the workup were inhibited by a combination of pH control with shock freezing and ultracentrifuging. These high-quality tuneable core–shell nanocomposite particles exhibit superparamagnetic character and sufficiently high magnetization with great potential for biomedical applications (e.g. MRI, cell separation and magnetically driven drug delivery systems) either as-prepared or by additional surface modification for improved biocompatibility.

Keywords Core–shell · Silica · Non-aggregated · Nanoparticle · Inverse microemulsion · Superparamagnetism · Nanomedicine

Electronic supplementary material The online version of this article (doi:10.1007/s11051-009-9661-7) contains supplementary material, which is available to authorized users.

C. Vogt · M. S. Toprak (✉) · M. Muhammed
Functional Materials Division, Royal Institute of Technology, 16440 Kista, Sweden
e-mail: toprak@kth.se

S. Laurent · J.-L. Bridot · R. N. Müller
Department of General, Organic, and Biomedical Chemistry, NMR and Molecular Imaging Laboratory, University of Mons-Hainaut, 7000 Mons, Belgium

Introduction

The necessity for synthesis of nanoparticles with well-controlled size and morphology emerged with the development in recent years of novel advanced applications such as biomedical related fields (including drug delivery (Douglas et al. 1987; Kaul and Amiji 2002; Levy et al. 2002; Xu et al. 2008), diagnostic (Rockall et al. 2005; Wheatley et al. 2006; Farrar et al. 2008), biomolecule separation and detection systems (Jing et al. 2007; Smith et al. 2007; Kist and Mandaji 2004; Fornara et al. 2008), data storage devices (Tanase et al. 2007; Hyun et al. 2007), skin-care products and dermatological formulations (Souto and Müller 2008; Nohynek et al. 2007; Popov et al. 2005), water purification systems (Li et al. 2008) etc. These applications also call for

nanoparticles with more complex architecture obtained by synthesis or post-synthesis procedures such as core–shell structures and multifunctional nanoparticles that can carry several components with different functionality.

Since the first article describing a method to synthesise magnetic nanoparticles (Massart 1981) was published, the interest in this type of nanoparticles increased. Several synthetic routes have been developed for their production including coprecipitation, polyol and microemulsion methods, high temperature decomposition of organic precursors, and spray/laser pyrolysis (Tartaj et al. 2003; Lu et al. 2007a, b; Laurent et al. 2008; Gupta and Gupta 2005) The thermal decomposition route based on iron oleate as a precursor is a technically easy, nontoxic and environmental-friendly route to produce high yield of iron oxide nanoparticles capped with oleic acid and with a finely tailored size from 5 nm to 22 nm (Park et al. 2004).

For applications in biology, medical diagnostics and therapy the superparamagnetic iron oxide nanoparticles (SPION) are desired (Tartaj et al. 2003; Rye 1996). Regardless of the application, in vivo or in vitro, SPION have to possess some basic properties, specifically: a size of less than 20 nm; high surface area with a larger platform for surface functionalisation; high colloidal stability; and the ability to pass the biological barriers (Kreyling et al. 2006). However, especially for the in vivo applications, the particles should adhere to more strict requirements: non-toxicity, non– immunogenicity, long-term retention within blood circulation, and the ability to reach and pass through the endothelial capillary membranes without embolism of the bigger vessels (Tartaj et al. 2003). These additional requirements directed the research towards the development of new preparation methods that produce magnetic nanoparticles with well-defined size, shape and high crystallinity.

However, even the new generation SPION with size monodispersity and special magnetic properties cannot be used as prepared, surface modification being a necessity not only to avoid agglomeration but also to increase the biocompatibility and the retention time in the blood stream. Coating with an additional layer is the most common approach to achieve these goals. Surface-modified SPION are FDA approved materials for biological applications (LaConte et al. 2005; Sosnovik et al. 2008). Among the coating materials studied are polymers including starch (Kim et al. 2003a, b), polyethylene glycol (PEG) (Kim et al. 2003a, b; Mikhaylova et al. 2004), dextran (Berry et al. 2004; Raynal et al. 2003), metal layers such as Au (Wang et al. 2005; Caruntu et al. 2005), and Ag (Mandal et al. 2005; Lai et al. 2005) or other inorganic materials such as silica. Silica is one of the preferred materials for coating the magnetic nanoparticles because of its high bio-stability, very low toxicity and versatile possibilities for surface functionalisation due to the exposed silanol groups.

Silica coating of the iron oxide nanoparticles can be performed by various synthetic routes among which the two most common routes are the Stöber method (Stoeber et al. 1968; Barnakov et al. 2005; Im et al. 2005; Lu et al. 2002; Deng et al. 2005) and microemulsion process (Santra et al. 2001; Lu et al. 2007a, b). The Stöber method, used mainly for the preparation of silica nanoparticles (Rao et al. 2005), is also applied for the formation of core–shell nanoparticles. The shell thickness can be controlled by the parameters that are involved in the process (temperature, concentration, time etc). Although the method is relatively simple, the core–shell nanoparticles synthesised by this method display multicored architecture with a non-uniform thickness of the silica, both important factors affecting their performance. The microemulsion method is an alternative to the Stöber method. Water-in-oil microemulsion (w/o), or inverse microemulsion, was studied and used extensively for synthesis of monodisperse silica nanoparticles (Yao et al. 2008; Osseo-Asare and Arriagada 1990; Arriagada and Osseo-Asare 1992; Arriagada and Osseo-Asare 1999; Arriagada and Osseo-Asare 1999; Osseo-Asare and Arriagada 1999). This route is also becoming increasingly favoured for the synthesis of core–shell complex structures and has recently been used for the production of core–shell iron oxide–silica nanoparticles (Lu et al. 2007a, b; Yi et al. 2006; Zhang et al. 2008; Yi et al. 2005; Narita et al. 2009). However, as for the case of silica nanoparticles synthesis, the microemulsion method produces core–shell nanoparticles strongly necked, due to the condensation reaction continuing during the separation process. In addition to this, an important part of the earlier reported particles are multicored core–shell nanoparticles. The formation of multicored nanoparticles and the strong

necking and aggregation of the synthesised nanoparticles result in increased overall size, decrease in the surface area and decreased stability in liquids. These drawbacks will hinder their potential use for in vivo and in vitro applications where an overall size less than 50 nm, high monodispersity, and non-aggregated nanoparticles are essential. In conclusion, to the best of our knowledge, until now the synthesis of well-dispersed, perfectly separated (without the presence of interparticle bridging) and single core–shell nanoparticles failed using either of the routes described above.

In this study, we report on preparation of single core iron oxide–silica shell nanoparticles with an excellent control of the shell thickness, high degree of separation and monodispersity, reaching up to a silica shell thickness of $\sim$13 nm (with the potential to further increase the shell thickness). Understanding the mechanism through which the process is taking place allowed us to precisely control the synthesis and obtain a very good reproducibility. The synthesis is based on a two-step method: (i) synthesis of oleic acid capped SPION core by thermal decomposition; (ii) silica coating on the core by the inverse microemulsion technique followed by new additional post synthesis steps for a successful separation. The influence of the stirring rate during the synthesis and the condensation time are investigated in order to finely tune the thickness of the silica shell of core-shell nanoparticles.

Experimental section

Materials

Sodium oleate (82%), $FeCl_3{\cdot}6H_2O$ (99%), 1-octadecene (90%), Triton-X100 (analytical grade), cyclohexane (99.5%) and hexanol (98%) were purchased from Sigma Aldrich and hexane (98.5%), oleic acid, tetraethyl orthosilicate (TEOS) (99.5%) and $NH_3{\cdot}H_2O$ (28%) from Fluka. The water used was MilliQ pure water with a resistivity of 18 MΩ, and ethanol was of 99.9% purity. All the chemicals were used as received without further purification.

Transmission electron microscopy (TEM) analyses of the nanoparticles' size and morphology were performed with JEOL 2100 at 200-kV acceleration. Samples for TEM study were prepared by dipping a carbon-coated TEM grid in sonicated particle suspension and allowing to dry at room temperature over night.

Fourier Transform Infrared Spectroscopy (FTIR) analysis of solid/liquid samples was performed using Nicolet Avatar IR 360 E.S.P. spectrophotometer and scans were performed in the range of 400–4,000 cm^{-1}.

Atomic absorption spectroscopy (AAS) for concentration determination was performed with Varian SpectrAA-220. Samples for AAS was prepared by dissolving a known volume of solution in acid under heating, and triplicate measurements were performed for concentration determination of the analyte.

The magnetization measurements were performed using a vibrating sample magnetometer, VSM (NUOVO MOLSPIN, UK) in the magnetic field range of $\pm$1 Tesla.

Methods

Synthesis of SPION

SPION were prepared by thermal decomposition of iron oleate in a high boiling point solvent (1-octadecene) through a two-step method described in detail elsewhere (Park et al. 2004; Qin et al. 2007). In a typical experiment, in the first step iron oleate was produced by reacting 40 mmols of $FeCl_3 \cdot 6H_2O$ with 120 mmols of sodium oleate in a solvent mixture composed of ethanol, distilled water and hexane in ratios: 4:3:7 (v/v/v). In order to obtain the SPION capped with oleic acid nanoparticles, the iron oleate was then decomposed at 320°C in 1–octadecene using oleic acid as capping agent. The resulting particles were washed by several cycles of precipitation, centrifugation and resuspension, successively, in ethanol and hexane to remove the unreacted precursors and impurities. FTIR analysis were performed on the SPION from cyclohexane to confirm the presence of oleic acid on the surface. Finally, the particles were resuspended in cyclohexane and kept at 4°C until further use.

SPION-silica core–shell nanoparticles:

The SiO_2-coated SPION were produced in an optimised inverse microemulsion Triton-X100/hexanol/water/cyclohexane system. In a typical experiment, the microemulsion was formed by mixing the magnetic

particles suspension in cyclohexane (0.89 mg Fe_3O_4 per 7 ml cyclohexane) with Triton-X100, hexanol, water, and $NH_3 \cdot H_2O$. After the formation of the microemulsion, TEOS was added drop wise and stirring continued for another 2 h. The formed core–shell particles were collected by destabilising the microemulsion via pH adjustment to ~ 2, alternating cycles of shock cooling in liquid N_2, centrifuging at high rpm and redispersing the collected particles in ethanol and finally in water. The particles in different stages of reaction were analysed by FTIR to assess/evidence the ligand exchange mechanism on the surface of the magnetic core. The particles were finally re-suspended in water and kept at 4°C until further use.

Results and discussions

The comprehension of the synthesis mechanism is essential for developing a successful and reproducible fabrication route with a high degree of control during the formation of the core–shell nanoparticles. Therefore, prior to detailing the results on the synthesis of SPION and SPION-silica nanoparticles, we present our findings on the mechanism.

Mechanism of silica coating on SPION

The oleic acid-coated SPION are easily dispersible in nonpolar media. The phase transfer of the SPION with hydrophobic ligands from the oil phase to the water phase (Darbandi et al. 2005; Liao et al. 2007) is essential for the formation of the core–shell architecture on the SPION core. This is a result of a ligand exchange on the surface of the SPION where hydrophobic ligands are replaced by the partially hydrolysed species of alkoxysilane. The ligand exchange mechanism has been proposed on a similar system: quantum dots coated with silica layer by inverse microemulsion method, first time by Darbandi (Darbandi et al. 2005) and more recently by Koole et al (Koole et al. 2008) but with no physical support was provided for the proposed exchange mechanism. FTIR spectra of oleic acid-capped magnetic nanoparticles before and after the addition of TEOS in the nanoparticles suspension are presented in Fig. 1. As seen, FTIR spectrum of oleic acid-capped nanoparticles exhibit characteristic peaks of carboxylic acid groups at 1380 cm^{-1} that are assigned to COOH group (Fig. 1, inset b) and at 2910 and 2840 cm^{-1} which are stretching vibrations of CH_3 and CH_2 groups in the carbon backbone (Fig. 1, inset a). SPION, after the addition of TEOS, exhibit new set of peaks that belong to Si–O–Si and Si–OH at 1150 cm^{-1} and 950 cm^{-1}, respectively (Fig. 1, inset b). The band observed at 2,345 cm^{-1}, after TEOS addition, is assigned to combination modes and overtones of SiO_2 glass matrix. These are strong evidences for the exchange of oleic acid ligands by silica bearing groups.

The three-stage mechanism (Scheme 1) that we suggest for the formation of iron oxide core–silica shell nanoparticles by inverse microemulsion is confirmed by the observed spectroscopical changes on SPION surface and by FTIR analyses following phase transfer of SPION for the formation of core–shell nanoparticles. In the initial stage the formation of the inverse microemulsion and stabilisation of

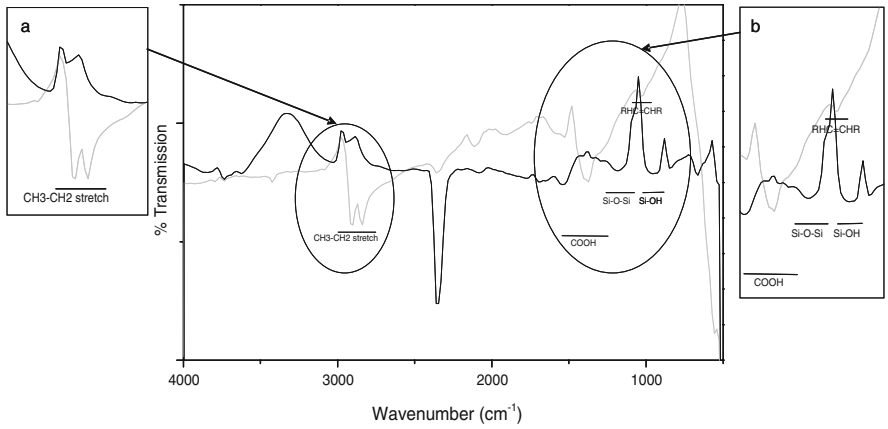

Fig. 1 FTIR spectra of the SPION capped with oleic acid before (*grey line*) and after (*black line*) the addition of TEOS

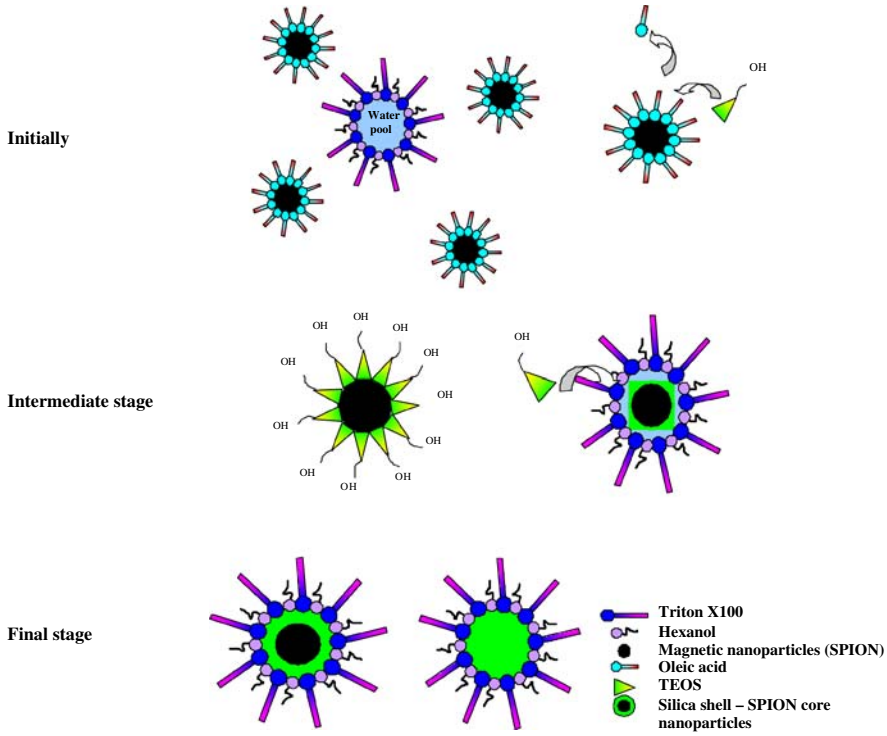

Scheme 1 Schematic description of mechanism of the SPION core-silica shell nanoparticle architecture formation after Darbandi (Darbandi et al. 2005)

water droplets by hexanol and Triton-X100 takes place. After the addition of TEOS, the hydrophobic ligands on the surface of SPION is exchanged by hydrolysed TEOS species. Consequently, the magnetic nanoparticles solubilized in oil phase are transferred into water phase. In an intermediate stage, the continuous association of the hydrolysed TEOS molecules in excess from the oil phase (Arriagada and Osseo-Asare 1999a, b) with the inverse micelles produces the condensation and growth of silica shells on the surface of the water phase-transferred SPION. In the final stage, core–shell nanoparticles with different silica shell thicknesses are obtained.

The SPION core and core–shell nanoparticles synthesis

SPION nanoparticles with an average particle size of 9.5 (±1.2) nm were successfully obtained by the described procedure. TEM images, presented in Fig. 2a, show that the particles have a narrow size distribution and are highly crystalline as observed

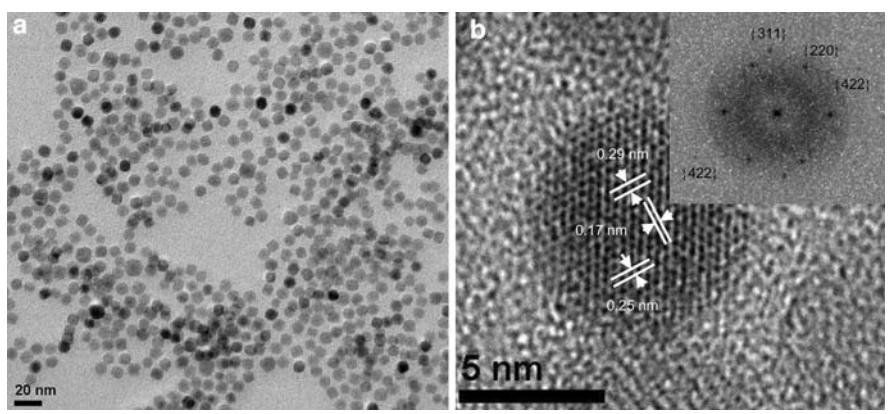

Fig. 2 TEM images of the core iron oxide nanoparticles synthesised by thermal decomposition method **a** low magnification, and **b** HRTEM of SPION. The insert represents FFT performed on a selected area within the crystalline region of SPION

from the HRTEM image (Fig. 2b). The *d* spacing from the HRTEM images correspond to the planes {220}, {331} and {422} of magnetite (or maghemite) crystal (ICDD#: 01-086-1358), also confirmed by XRD analysis (Fig. S1a). The average crystallite size was also calculated from XRD measurements, using Scherrer's equation and a value of 10.5 nm was obtained. The oleic acid capping was confirmed by the FTIR spectrum presented in Fig. 1.

The SPION were used as core for the fabrication of core–shell nanocomposites in an inverse (w/o) microemulsion Triton-X100/hexanol/water/cyclohexane system. In this method, the continuous phase (oil phase) consisted of cyclohexane and Triton-X100/hexanol is the surfactant/co-surfactant couple. SPION are easily dispersible in cyclohexane due to the hydrophobic oleic acid capping. According to the mechanism presented above, the oleic acid capping of the SPION is particularly important for the ligand exchange to take place on the surface of the magnetic core. This will result in a controlled phase transfer of the cores in the water droplets of the dispersed phase and homogeneous silica coating. The amount of magnetic particles in microemulsion has to be adjusted to ensure the formation of single core coated with silica layer with no silica nanoparticles or multicored beads being formed. Several experiments have been performed to obtain a stability region where this microemulsion system can be used reliably and reproducibly. Our survey of varying concentrations yielded the following values for the molar ratio of components: H_2O/Triton-X100: 6.3; Triton-X100/hexanol: 0.5; and TEOS/ H_2O: 0.008.

A representative TEM image of core–shell nanoparticles is given in Fig. 3, showing that the magnetic core is highly crystalline and the silica shell is amorphous—as no regular crystallographic planes were observed and electron diffractogram obtained from the shell had no indication of crystallinity.

In our study of optimising and controlling the synthetic process for the formation of the silica layer, we evaluated the influence of various experimental parameters: the effect of the stirring rate, the reaction time and the post-synthesis washing steps.

The stirring rate was varied from 400 rpm to 1,200 rpm, and it was found that this only had a minimum influence on the size dispersion and homogeneity of core–shell nanoparticles. At all stirring rates, the formation of single core SPION-silica shell nanoparticles took place with no empty silica particles being observed (Fig. S2). The stirring rate plays an important role of keeping the microemulsion system stable. At low stirring rate (from 400 up to 600 rpm), a high percentage of the core–shell particles formed in the system were attaching to the glass walls. At higher stirring rates, this fact was not observed probably because the stirring speed was high enough to overcome the physical interactions between the newly formed particles and the reactor's walls. Images of silica shell growth after 2 h of stirring at different rates are presented in Fig. 4: at all stirring rates, the overall size of SPION-silica nanoparticles remains constant with a slight increase in the size and polydispersity at higher stirring rates.

For some high-end applications, including biomedical, it is very important to precisely control the thickness of the silica shell. Therefore we investigated the variation of silica shell thickness as a function of time, where the amount of TEOS and the SPION core size were maintained constant. Figure 5, represents a series of TEM images of the particles obtained after different reaction durations (from 2 to 26 h). A closer investigation of the TEM images complemented by the SEM images of the same particles (Fig. S3) reveals the fact that even after a short reaction time of 2 h the silica shell has a considerable thickness of 5.2 ± 1.7 nm. The

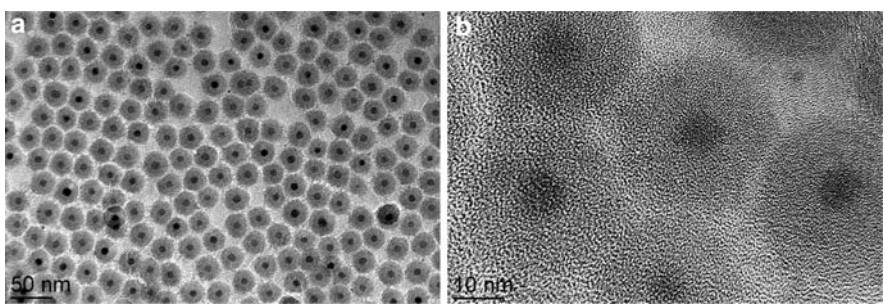

Fig. 3 **a** TEM and **b** HRTEM images of a typical sample of SPION core–silica shell nanoparticles

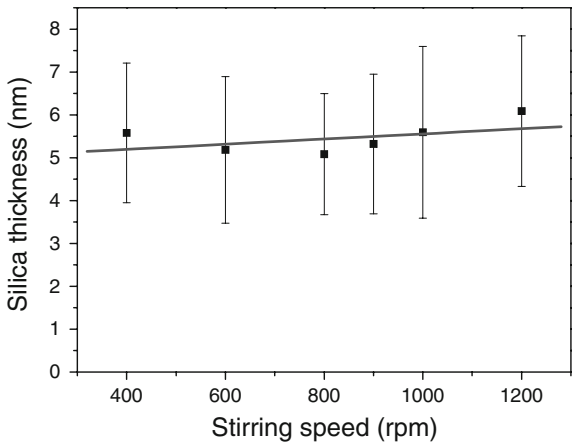

Fig. 4 Size dependence of the core–shell nanoparticles on the stirring rate for reaction duration of 2 h (the continuous line represents the data trend)

thickness of the silica shell for the adopted set of initial conditions increases linearly with time and reaches a value of 10.5 ± 1.9 nm after 17 h, whereafter it remains almost constant even if the reaction time is further increased. This is attributed to the slow reaction kinetics due to the low amount of the remaining TEOS. Measurements of the thickness of the silica shell in time course experiments are summarised in Fig. 6a. Furthermore, the core–shell nanoparticles in microemulsion can still be active nucleation sites for the formation of new silica layer. Experiments performed by the addition of fresh TEOS after the stabilisation of the size increase the thickness of the silica shell (13.2 ± 1.92 nm) further, without destabilising the microemulsion. Representative TEM image of the sample after extra addition of TEOS is presented in Fig. S4.

Magnetic measurements of the SPION and core–shell nanocomposites by VSM analysis is presented in Fig. 6b which shows that the particles are superparamagnetic (SPION) with a saturation magnetisation (Ms) of 81 emu/g and no coercivity. The magnetic core size calculated from VSM (9.5 nm) is the same for all the samples in good agreement with value obtained from TEM demonstrating that iron oxide nanoparticles are single crystalline. This also shows that surface of the SPION core is not influenced during the coating process. The core-shell nanocomposites retained the superparamagnetic character of the magnetic core particles, with the normalised Ms values (expressed in emu per unit weight of core–shell sample) of 17.6, 11.28, and 7.3 emu/g for

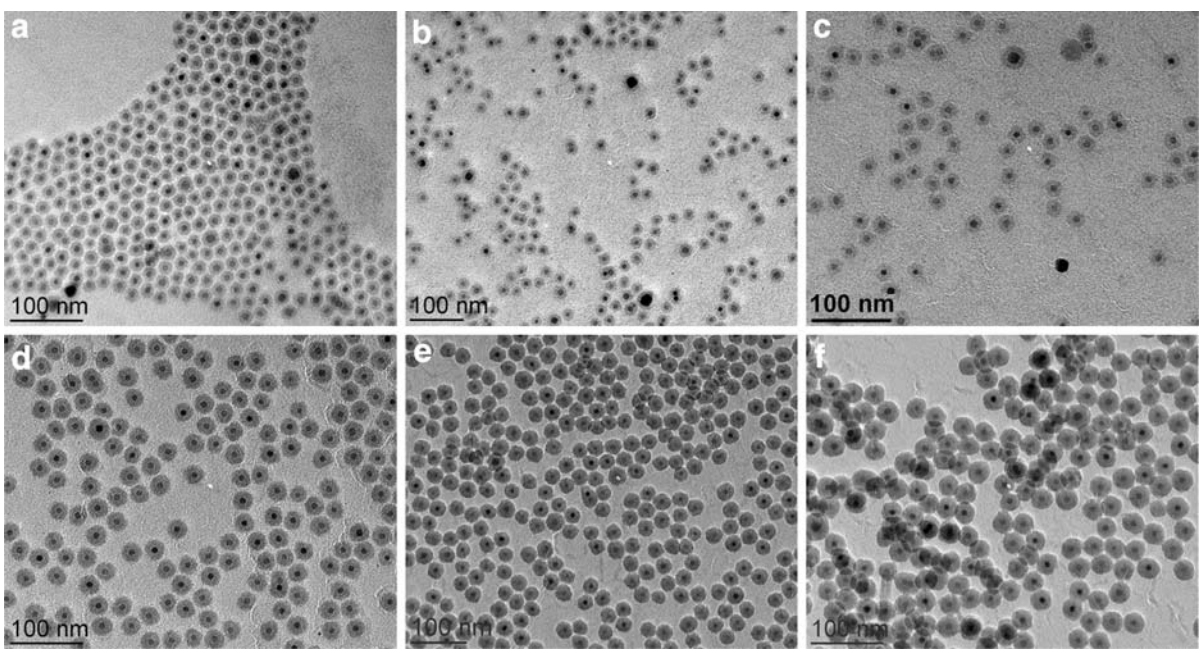

Fig. 5 TEM images of the SPION core–silica shell nanoparticles with various silica shell thickness: **a** 5.2 ± 1.7 nm; **b** 5.7 ± 1.1 nm; **c** 6.1 ± 1.1 nm; **d** 9 ± 1.8 nm; **e** 10.5 ± 1.9 nm; and **f** 10.4 ± 1.8 nm

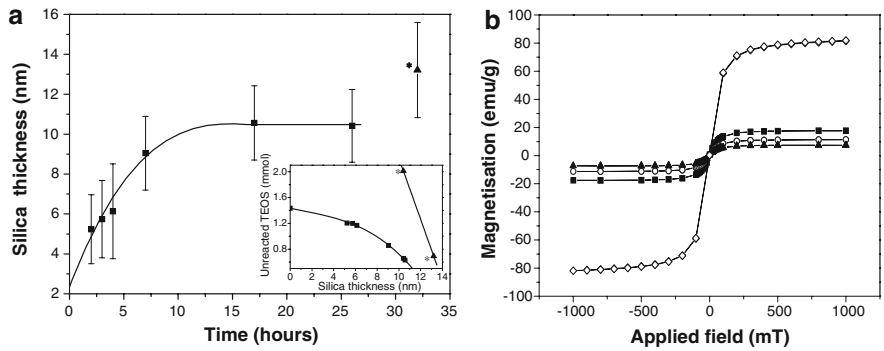

Fig. 6 **a** Silica layer thickness of SPION core-silica shell nanoparticles as a function of time. The inset represents the silica layer thickness as a function of unreacted TEOS in the microemulsion (the continuous line represents the data trend). The point * indicates the addition of extra TEOS after the maximum size is reached for the initially adopted conditions; **b** Magnetic measurements on the core (*diamond*) and core-shell nanocomposite spheres performed by VSM with a silica thickness of ~5.2 nm (*filled square*), ~8.6 nm (*circle*) and ~10.5 nm (*filled triangle*)

the samples coated with silica layer thickness of ~5.2 nm, ~8.6 nm and ~10.5 nm corresponding to 2, 6 and 17 h reaction time, respectively. Magnetisation per unit weight of sample decreases as the thickness of the silica shell increased for the same magnetic core size of SPION. These nanocomposite structures are sufficiently magnetically responsive for medical imaging or targeted drug delivery applications.

In a further step to assess the density of silica coating layer, we performed leaching experiments where core–shell nanoparticles with different shell thicknesses were treated with a concentrated solution of HCl for 5 min. Resulting structures, presented in Fig. 7, revealed that the silica layer is porous enough to allow access of the acid to the SPION core and enable it to be dissolved completely. Similar hollow structures were reported earlier by Mornet et al (Mornet et al. 2002) upon dissolving the core. The porosity of the silica shell can be used as a matrix on/in which therapeutics can be adsorbed and be released via local heat generated in the core (due to SPION) using AC magnetic field or pH change in the environment. We utilised the porous silica layer to load pH sensitive dye molecules as model drug and controlled their release with pH (data not shown). Partially dissolved cores with different shapes were also obtained when diluted HCl was used (Yi et al. 2006). Hollow, porous and intact silica spheres obtained by HCl treatment are interesting structures which could be used for confined zone synthesis within silica capsules or for controlled drug release induced by the thickness of the silica shell. Extended exposure to acid had no effect on the hollow silica structures.

Moreover, we addressed the problem of aggregation and agglomeration of the particles obtained by microemulsion process. The microemulsion synthesis process currently has limitations. Firstly, the yield of the synthesis process is relatively low. Secondly, the resulting core–shell nanocomposites are strongly necked which indicates the existence of residual reactions leading to formation of silica layer connecting particles together, as previous reports on

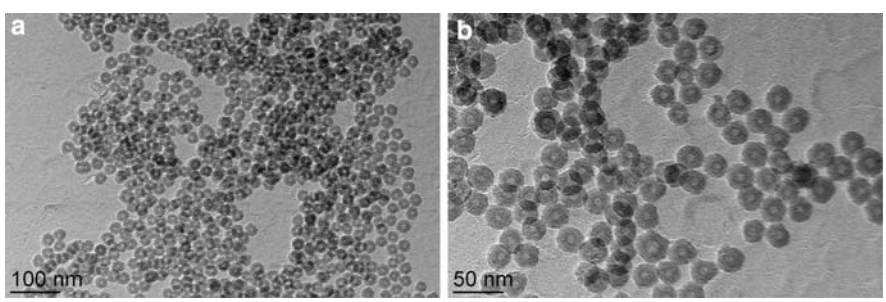

Fig. 7 TEM images of the core –shell nanoparticles with silica shell thickness of **a** ~9 nm, **b** ~10.5 nm after treatement with conc. HCl

core–shell nanocomposites (Santra et al. 2001; Lu et al. 2007a, b; Yi et al. 2006; Zhang et al. 2008; Yi et al. 2005; Narita et al. 2009) showed. While the problem of low yield of the procedure is difficult to solve, due to low concentration of the reactants, eliminating the interparticle bridging is approachable. Therefore, we investigated modifications to the post-synthesis pathway which led to solve the necking and irreversible agglomeration problems of nanoparticles in the separation process. Processing methods like already described (Lu et al. 2007a, b; Yi et al. 2006; Zhang et al. 2008; Yi et al. 2005; Narita et al. 2009; Mornet et al. 2002) such as alternating cycles of ethanol or acetone addition for destabilising the microemulsion and centrifuging or diluting the system with an excess of solvent (cyclohexane) did not produce separated nanoparticles. Introducing a combination of two new steps in the separation process resulted in dramatically improved quality of particles with no aggregation or necking retention. (i) The pH adjustment of the aqueous phase in the pH range of 1–2 (Brinker and Sherer 1990) minimised the condensation rate of TEOS. (ii) The kinetic destabilization of the microemulsion by shock cooling the solution results in phase separation, thereby slowing down the reaction and making the separation of nanoparticles from the remaining unreacted precursor much more easy. With this procedure, we successfully manufactured highly separated, non-aggregated magnetic core–silica shell nanoparticles.

Conclusions

In this study, we presented an optimised inverse microemulsion method for finely tuneable shell core–shell nanoparticle synthesis intended for biomedical applications. We successfully synthesised core–shell nanoparticles having a narrow size distribution with a crystalline magnetic core and a tuneable amorphous, porous silica shell thickness ($\sim$5–13 nm silica shell thickness) with possibility of increasing the size of the overall particles by adjusting the amount of silica precursor. The transfer of the SPION from the oil phase to the water phase through a ligand exchange mechanism is evidenced by FTIR spectra. The phase transfer mechanism is experimentally confirmed by the monodispersed size—single central core–silica shell adjustable thickness core—shell nanoparticles resulting from this synthesis. With the carefully adjusted post-synthesis processing procedures (pH adjustment to the region of minimum condensation of TEOS and shock cooling the solution that results in phase separation), the produced core–shell nanoparticles are highly separated, with no residual aggregation. Magnetic measurements performed on the fabricated SPION core and core–shell nanoparticles showed a superparamagnetic character with sufficiently high magnetization, rendering them useful for biomedical applications. Although the amount of material to be synthesized in one batch of microemulsion process is limited (a characteristic of the method as the initial concentration of the reactants is low), for highly specialized and high impact applications, such as biomedical targeting and imaging (e.g. magnetically driven drug delivery systems, MRI contrast agents, cell separation, etc.), small quantities of samples with very high quality are required. Most important requirements for biomedical applications are very well achieved by the characteristics of presented core–shell nanoparticles: an overall size under 50 nm with a controllable thickness of biocompatible silica shell in the form of completely non-aggregated, single core nanocomposites and stable suspension.

Acknowledgements This study is partially funded by the European Commission sixth Framework Program (INNOMED LSHB-CT-2005-518170), FNRS, the FP7 (ENCITE Program) and the ARC Program 05/10-335 of the French Community of Belgium. MST acknowledges the fellowship from Knut and Alice Wallenberg's Foundation (No:UAW2004.0224).

References

Arriagada FJ, Osseo-Asare K (1992) Phase and dispersion stability effects in the synthesis of silica nanoparticles in a non-ionic reverse microemulsion. Colloids Surf 69:105–115

Arriagada FJ, Osseo-Asare K (1999a) Controlled hydrolysis of tetraethoxysilane in a nonionic water-in-oil microemulsion: a statistical model of silica nucleation. Colloids Surf A 154:311–326

Arriagada FJ, Osseo-Asare K (1999b) Synthesis of nanosize silica in a nonionic water-in-oil microemulsion: effects of the water/surfactant molar ratio and ammonia concentration. J Colloid Interface Sci 211:210–220

Barnakov YA, Yu MH, Rosenzweig Z (2005) Manipulation of the magnetic properties of magnetite–silica nanocomposite materials by controlled Stober synthesis. Langmuir 21:7524–7527

Berry CC, Wells S, Charles S, Aitchison G, Curtis ASG (2004) Cell response to dextran-derivatized iron oxide nanoparticles post internalization. Biomaterials 25:5405–5413

Brinker JC, Sherer GW (1990) Sol-gel science. The physics and chemistry of sol-gel processing. Academic Press, San Diego

Caruntu D, Cushing BL, Caruntu G, O'Connor CJ (2005) Attachment of gold nanograins onto colloidal magnetite nanocrystals. Chem Mater 17:3398–3402

Darbandi M, Thomann R, Nann T (2005) Single quantum dots in silica spheres by microemulsion synthesis. Chem Mater 17:5720–5725

Deng Y-H, Wang C-C, Hu J-H, Yang W-L, Fu S-K (2005) Investigation of formation of silica-coated magnetite nanoparticles via sol-gel approach. Colloids Surf A 262: 87–93

Douglas SJ, Davis SS, Illum L (1987) Nanoparticles in drug delivery. Crit Rev Ther Drug Carr Syst 3:233–261

Farrar CT, Dai G, Novikov M, Rosenzweig A, Weissleder R, Rosen BR, Sosnovik DE (2008) Impact of field strength and iron oxide nanoparticle concentration on the linearity and diagnostic accuracy of off-resonance imaging. NMR Biomed 21:453–463

Fornara A, Johansson P, Petersson P, Gustafsson S, Qin J, Olsson E, Ilver D, Krozer A, Muhammed M, Johansson C (2008) Tailored magnetic nanoparticles for direct and sensitive detection of biomolecules in biological samples. Nano Lett 8:3423–3428

Gupta AK, Gupta M (2005) Synthesis and surface engineering of iron oxide nanoparticles for biomedical applications. Biomaterials 26:3995–4021

Hyun C, Lee DC, Korgel BA, Ad Lozanne (2007) Micromagnetic study of single-domain FePt nanocrystals overcoated with silica. Nanotechnology 18:055704–055711

Im SH, Herricks T, Lee YT, Xia Y (2005) Synthesis and characterization of monodisperse silica colloids loaded with superparamagnetic iron oxide nanoparticles. Chem Phys Lett 401:19–23

Jing Y, Moore LR, Williams PS, Chalmers JJ, Farag SS, Bolwell B, Zborowski M (2007) Blood progenitor cell separation from clinical leukapheresis product by magnetic nanoparticle binding and magnetophoresis. Biotechnol Bioeng 96:1139–1154

Kaul G, Amiji M (2002) Long-circulating poly(ethylene glycol)-modified gelatin nanoparticles for intracellular delivery. Pharm Res 19:1061–1067

Kim DK, Mikhaylova M, Wang FH, Kehr J, Bjelke B, Zhang Y, Tsakalakos T, Muhammed M (2003a) Starch-coated superparamagnetic nanoparticles as MRI contrast agents. Chem Mater 15:4343–4351

Kim DK, Mikhaylova M, Zhang Y, Muhammed M (2003b) Protective coating of superparamagnetic iron oxide nanoparticles. Chem Mater 15:1617–1627

Kist TBL, Mandaji M (2004) Separation of biomolecules using electrophoresis and nanostructures. Electrophoresis 25:3492–3497

Koole R, van Schooneveld MM, Hilhorst J, de Mello Donegá C, Hart DC, van Blaaderen A, Vanmaekelbergh D, Meijerink A (2008) On the incorporation mechanism of hydrophobic quantum dots in silica spheres by a reverse microemulsion method. Chem Mater 20:2503–2512

Kreyling WG, Semmler-Behnke M, Moeller W (2006) Health implications of nanoparticles. J Nanopart Res 8:543–562

LaConte L, Nitin N, Bao G (2005) Magnetic nanoparticle probes. Mater Today 8:32–38

Lai C-H, Wu T-F, Lan M-D (2005) Synthesis and property of core-shell Ag@Fe3O4 nanoparticles. IEEE Trans Magn 41:3397–3399

Laurent S, Forge D, Port M, Roch A, Robic C, Vander Elst L, Muller RN (2008) Magnetic iron oxide nanoparticles: synthesis, stabilization, vectorization, physicochemical characterizations, and biological applications. Chem Rev 108:2064–2110

Levy L, Sahoo Y, Kim K-S, Bergey EJ, Prasad PN (2002) Nanochemistry: synthesis and characterization of multifunctional nanoclinics for biological applications. Chem Mater 14:3715–3721

Li Q, Mahendra S, Lyon DY, Brunet L, Liga MV, Li D, Alvarez PJJ (2008) Antimicrobial nanomaterials for water disinfection and microbial control: potential applications and implications. Water Res 42:4591–4602

Liao Y, Li W, He S (2007) Properties of CdSe quantum dots coated with silica fabricated in a facile way. Nanotechnology 18:375701–375705

Lu Y, Yin Y, Mayers BT, Xia Y (2002) Modifying the surface properties of superparamagnetic iron oxide nanoparticles through a sol-gel approach. Nano Lett 2:183–186

Lu A-H, Salabas EL, Schueth F (2007a) Magnetic nanoparticles: synthesis, protection, functionalization, and application. Angewandte Chemie, Int Edn 46:1222–1244

Lu C-W, Hung Y, Hsiao J-K, Yao M, Chung T-H, Lin Y-S, Wu S-H, Hsu S-C, Liu H-M, Mou C-Y, Yang C-S, Huang D-M, Chen Y-C (2007b) Bifunctional magnetic silica nanoparticles for highly efficient human stem cell labeling. Nano Lett 7:149–154

Mandal M, Kundu S, Ghosh SK, Panigrahi S, Sau TK, Yusuf SM, Pal T (2005) Magnetite nanoparticles with tunable gold or silver shell. J Colloid Interface Sci 286:187–194

Massart R (1981) Preparation of aqueous magnetic liquids in alkaline and acidic media. IEEE Trans Magn MAG-17:1247–1248

Mikhaylova M, Kim DK, Bobrysheva N, Osmolowsky M, Semenov V, Tsakalakos T, Muhammed M (2004) Superparamagnetism of magnetite nanoparticles: dependence on surface modification. Langmuir 20:2472–2477

Mornet S, Grasset F, Portier J, Duguet E (2002) Maghemite@Silica nanoparticles for biological applications. Eur Cells Mater 3:110–113

Narita A, Nakab K, Chujo Y (2009) Facile control of silica shell layer thickness on hydrophilic iron oxide nanoparticles via reverse micelle method. Colloids Surf A 336: 46–56

Nohynek GJ, Lademann J, Ribaud C, Roberts MS (2007) Grey goo on the skin? Nanotechnology, cosmetic and sunscreen safety. Crit Rev Toxicol 37:251–277

Osseo-Asare K, Arriagada FJ (1990) Preparation of silica nanoparticles in a non-ionic reverse micellar system. Colloids Surf 50:321–339

Osseo-Asare K, Arriagada FJ (1999) Growth kinetics of nanosize silica in a nonionic water-in-oil microemulsion: a reverse micellar pseudophase reaction model. J Colloid Interface Sci 218:68–76

Park J, An K, Hwang Y, Park J-G, Noh H-J, Kim J-Y, Park J-H, Hwang N-M, Hyeon T (2004) Ultra-large-scale syntheses of monodisperse nanocrystals. Nat Mater 3:891–895

Popov AP, Priezzhev AV, Lademann J, Myllylä R (2005) TiO2 nanoparticles as an effective UV-B radiation skin-protective compound in sunscreens. J Phys D 38:2564–2570

Qin J, Laurent S, Jo YS, Roch A, Mikhaylova M, Bhujwalla ZM, Muller RN, Muhammed M (2007) A high-performance magnetic resonance imaging T2 contrast agent. Adv Mater 19:1874–1878

Rao KS, El-Hami K, Kodaki T, Matsushige K, Makino K (2005) A novel method for synthesis of silica nanoparticles. J Colloid Interface Sci 289:125–131

Raynal I, Prigent P, Peyramaure S, Najid A, Rebuzzi C, Corot C (2003) Macrophage endocytosis of superparamagnetic iron oxide nanoparticles: mechanisms and comparison of ferumoxides and ferumoxtran-10. Investig Radiol 39:56–63

Rockall AG, Sohaib SA, Harisinghani MG, Babar SA, Singh N, Jeyarajah AR, Oram DH, Jacobs IJ, Shepherd JH, Reznek RH (2005) Diagnostic performance of nanoparticle-enhanced magnetic resonance imaging in the diagnosis of lymph node metastases in patients with endometrial and cervical cancer. J Clin Oncol 23:2813–2821

Rye PD (1996) Sweet and sticky: carbohydrate-coated magnetic beads. Bio/Technology 14:155–157

Santra S, Tapec R, Theodoropoulou N, Dobson J, Hebard A, Tan W (2001) Synthesis and characterization of silica-coated iron oxide nanoparticles in microemulsion: the effect of nonionic surfactants. Langmuir 17:2900–2906

Smith JE, Medley CD, Tang Z, Shangguan D, Lofton C, Tan W (2007) Aptamer-conjugated nanoparticles for the collection and detection of multiple cancer cells. Anal Chem 79:3075–3082

Sosnovik DE, Nahrendorf M, Weissleder R (2008) Magnetic nanoparticles for MR imaging: agents, techniques and cardiovascular applications. Basic Res Cardiol 103:122–130

Souto EB, Müller RH (2008) Cosmetic features and applications of lipid nanoparticles (SLN®R, NLC®R). Int J Cosmet Sci 30:157–165

Stoeber W, Fink A, Bohn E (1968) Controlled growth of monodisperse silica spheres in the micron size range. J Colloid Interface Sci 26:62–69

Tanase M, Zhu J-G, Liu C, Shukla N, Klemmer TJ, Weller D, Laughlin DE (2007) Structure optimization of FePt nanoparticles of various sizes for magnetic data storage. Metall Mater Trans A 38A:798–810

Tartaj P, Del Puerto Morales M, Veintemillas-Verdaguer S, Gonzalez-Carreno T, Serna CJ (2003) The preparation of magnetic nanoparticles for applications in biomedicine. J Phys D 36:R182–R197

Wang L, Luo J, Fan Q, Suzuki M, Suzuki IS, Engelhard MH, Lin Y, Kim N, Wang JQ, Zhong C-J (2005) Monodispersed core-shell Fe3O4@Au nanoparticles. J Phys Chem B 109:21593–21601

Wheatley MA, Forsberg F, Dube N, Patel M, Oeffinger BE (2006) Surfactant-stabilized contrast agent on the nanoscale for diagnostic ultrasound imaging. Ultrasound Med Biol 32:83–93

Xu ZP, Niebert M, Porazik K, Walker TL, Cooper HM, Middelberg APJ, Gray PP, Bartlett PF, Lu GQ (2008) Subcellular compartment targeting of layered double hydroxide nanoparticles. J Control Release 130:86–94

Yao L, Xu G, Dou W, Bai Y (2008) The control of size and morphology of nanosized silica in Triton X-100 based reverse micelle. Colloids Surf A 316:8–14

Yi DK, Selvan ST, Lee SS, Papaefthymiou GC, Kundaliya D, Ying JY (2005) Silica-coated nanocomposites of magnetic nanoparticles and quantum dots. J Am Chem Soc 127:4990–4991

Yi DK, Lee SS, Papaefthymiou GC, Ying JY (2006) Nanoparticle architectures templated by SiO2/Fe2O3 nanocomposites. Chem Mater 18:614–619

Zhang M, Cushing BL, O'Connor CJ (2008) Synthesis and characterization of monodisperse ultra-thin silica-coated magnetic nanoparticles. Nanotechnology 19:085601–085605